The Frequency Fluctuation Impact Analysis for Droop Controlled Grid-connecting Inverter in Microgrid

Wei, Feng ; Sun, Kai; Guan, Yajuan; Guerrero, Josep M.; Xiao, Xi

Published in:
2016 8th International Power Electronics and Motion Control Conference - ECCE Asia (IPEMC 2016-ECCE Asia)

DOI (link to publication from Publisher):
10.1109/IPEMC.2016.7512890

Publication date:
2016

Document Version
Early version, also known as pre-print

The Frequency Fluctuation Impact Analysis for Droop Controlled Grid-connecting Inverter in Microgrid

Wei Feng[1], Kai Sun[1], Yajuan Guan[2], Josep M. Guerrero[2], Xi Xiao[1]
1) State Key Lab of Power Systems, Department of Electrical Engineering, Tsinghua University, Beijing, China,
2) Department of Energy Technology Department, Aalborg University, Aalborg, Denmark.
fwqqrse@163.com

***Abstract*—No matter with PV or batteries as DC source, the droop controlled grid-connecting inverter (DC-GCI) has been widely used in microgrid. As the bandwidth of the outer active and reactive power control loop is designed to be much slower when comparing to the inner voltage/current loop of the DC-GCI, and the low equivalent impedance presented by the system, the power disturbance resulting from grid's frequency fluctuation of DC-GCI may not be compensated by the outer power controller in time. Therefore, the frequency stability of the system mainly depends on its voltage tracking performance dominated by the inner loop's voltage control strategy. In this paper, three widely used inner voltage/current control schemes, including PI controller in the synchronous rotating reference frame, and the PR controller with fixed and dynamic resonant frequency in the stationary frame have been discussed. The small signal state space models of the system connected to the grid with different inner loop control schemes are established and compared. The conclusion is derived through the parameter sensitivity analysis. Finally, the simulation and experiment results from a scaled-down laboratory prototype have been presented to verify the validity of the conclusion.**

Keywords—Grid-connecting inverter; droop control; frequency fluctation; stability analysis

I. INTRODUCTION

NOWADAYS, there has been a significant change in the power system operation and planning, caused by environmental issues, uncertainty of the prices for fossil fuels, concerns about the security of supply [1]-[2]. The emergence of small-scale distributed and different type generators together with the present communication technology has created new opportunities for the operation of on-site hybrid power generation [3].

One promising power architecture is the microgrid (MG), which usually involves different kinds of energy sources, such as wind or photovoltaic (PV), etc. As a large number of power electronics interfaced distributed generations (DGs) units have been installed in the low-voltage power distribution system [4]-[5]. Then the stability problem is emerging. As a consequence, the performance of DG systems must be improved to meet the grid codes in each country [6].

With the renewable energy as DC source, the widely used conventional grid-connected current controlled inverter (GC-CCI) with maximum power point tracking (MPPT) have many advantages because of the high output impedance presented by GC-CCI [7], including easy to control and the high power quality of the grid-connecting current. However, the random irradiation or wind speed may become the disturbance to the grid utility as the penetration of renewable energy based GC-CCI increasing [8], especially in the small scale and islanded hybrid MG.

In order to overcome conventional GC-CCI's disadvantage, the droop controlled grid-connecting inverter (DC-GCI) is proposed in [9]-[10]. The DC-GCI injects the active and reactive power through controlling the amplitude and phase of its output voltage according to the droop law. Therefore, the system can participate in the grid's frequency and amplitude regulation, which will give a chance to improve the grid utility's damping performance. However, the low equivalent impedance presented by DC-GCI makes it vulnerable to the grid's voltages disturbance.

As the nonlinear loads increasing along the distribution line, the power quality of system's grid-connecting current will be deteriorated more easily by the grid's voltage at the point of common couple (PCC). Therefore, a harmonic grid-connecting current suppression strategy of DC-GCI is discussed in [11-12]. The regular multiple PR controllers are used as voltage controller to deal with harmonic current issue in [11]. The fundamental components is abstracted from distorted grid voltage through the filter, and then a hybrid voltage controller with PIR regulators in the *dq* frame is adopted for improving the voltage tracking capability of the grid harmonic voltage component at the PCC to suppress the harmonic current [12].

As the inevitable frequency fluctuation resulting from the dynamic loads disturbance and the dynamic response of the synchronous generator's governor [13]-[14], there is another issue for DC-GCI when adopting it in the regular power plant based islanded MG, and more challenges to the stability of hybrid MG arise. The main reason of the potential instability is the bandwidth of the DC-GCI's power flow control loop is usually designed to be much slower than its inner voltage/current loop, and the low equivalent output impedance presented by system [15]-[16], the disturbance of the system's output grid-connecting current may not be compensated by the

978-1-5090-1210-7/16/$31.00 ©2016 IEEE

power controller in time when the grid's frequency fluctuation occurred. Therefore, the frequency stability of the system mainly depends on its voltage tracking performance dominated by the inner loop's voltage control strategy.

In this paper, three widely used inner voltage/current control strategy, including PI controller in the synchronous rotating reference frame, and the PR controller with fixed and dynamic resonant frequency in the stationary frame have been discussed. The small signal state space models of the system with different inner voltage control schemes are established and compared. Then, the conclusion is derived through the parameter sensitivity analysis. Finally, the simulation and experiment results from a scaled-down laboratory prototype have been presented to verify the validity of the conclusion.

II. The Droop Controlled Grid-connecting Inverter In the Islanded Microgrid

A. The feature and configuration of islanded microgrid

In this paper, the objective islanded MG is established by a regular power system to supply the regular loads, for example, hydropower plant or diesel generator, as shown in Fig.1. Each DC-GCI is connected with sensitive local load and powered by energy storing system (ESS) system, which is charged by renewal energy, e.g. PV cell. The DC/DC converter with MPPT algorithm is used for maintaining batteries of ESS and controlling PV penal to output power as much as possible. The DC-GCI operate in the grid-connecting mode and injects dispatched active and reactive to the grid utility when the grid is normal. When grid fault occurred, the systems are disconnected from the grid and continue to supply the sensitive load for improving the reliability.

As the capacity of regular power station is much greater than the other renewable energy based DG units in the islanded MG, the voltage frequency and amplitude of the AC bus is dominated by the feature of governor and excitation system. Because of the governor and synchronous generator's huge inertia, it will take long time for governor to be stabilized when a great active loads step disturbance occurred, which means the frequency in objective MG will fluctuate a lot when comparing to the conventional stiff grid utility. A frequency and active power disturbance simulation of hydropower station based islanded MG is shown in Fig.2.

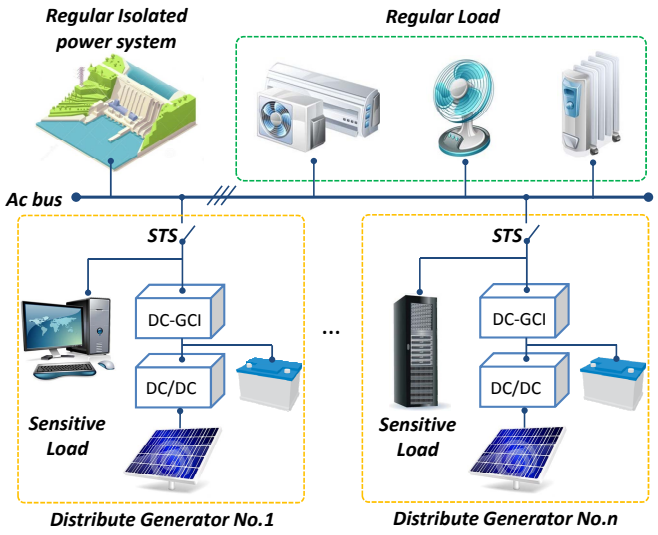

Fig. 1. The structure of islanded MG with DC-GCIs

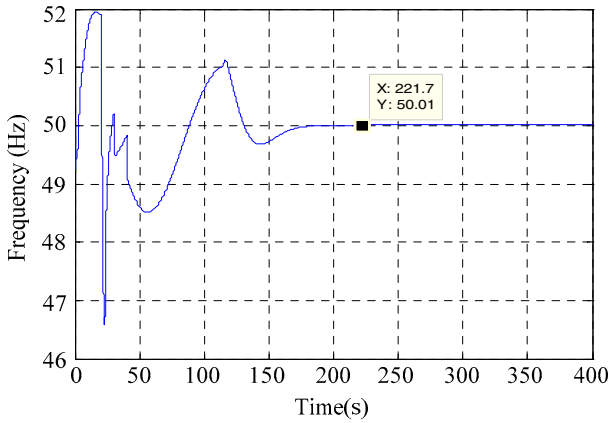

Fig. 2. The simulation of active power/frequency response in the islanded MG's established by hydropower station

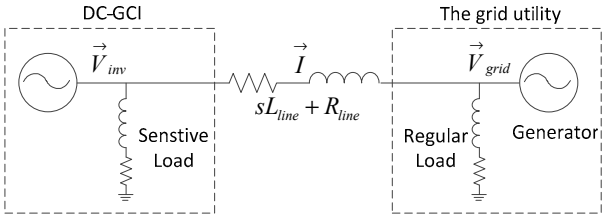

Fig.3. The simplified model of DC-GCI connecting with the grid

B. The power transfer principle of DC-GCI

The model of DC-GCI connecting with the grid utility can be simplified to two voltage sources with equivalent output impedance and are paralleled with line impedance, as shown in Fig. 3. The active and reactive power transferred from DC-GCI to the grid utility can be calculated as following:

$$\begin{cases} P = \dfrac{V_{\text{inv}} V_{\text{grid}}}{Z}\cos(\Delta\phi - \theta) - \dfrac{V_{\text{grid}}^{\ 2}}{Z}\cos(\Delta\phi) \\ Q = \dfrac{V_{\text{inv}} V_{\text{grid}}}{Z}\sin(\Delta\phi - \theta) - \dfrac{V_{\text{grid}}^{\ 2}}{Z}\sin(\Delta\phi) \end{cases} \quad (1)$$

Being P and Q are the transferred active and reactive power between two voltage source, V_{inv} and V_{grid} are amplitude of output voltage of DC-GCI and the grid utility, $\Delta\phi$ represents the phase between voltage vector $\boldsymbol{V}_{\text{inv}}$ and $\boldsymbol{V}_{\text{grid}}$. Z and θ are the module and angle of line impedance.

When line impedance is mainly inductive, θ is close to $\pi/2$, (1) can be simplified to (2), as shown follows:

$$\begin{cases} P = \dfrac{V_{\text{inv}} V_{\text{grid}}}{Z}\sin\Delta\phi \\ Q = \dfrac{V_{\text{inv}} V_{\text{grid}}\cos\Delta\phi - V_{\text{grid}}^{\ 2}}{Z} \end{cases} \quad (2)$$

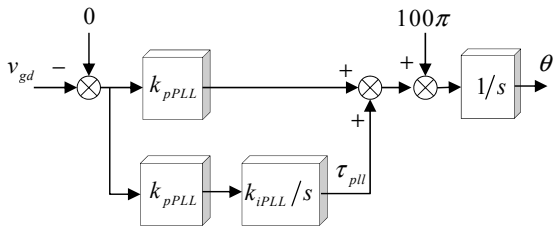

Fig. 4. The equivalent model of SRF-PLL

Therefore, the grid-connecting active and reactive power can be controlled by phase and amplitude difference between the output voltage of DC-GCI and the grid voltage at PCC.

III. Small Signal State Space Model and Frequency Stability Analysis

The DC-GCI can be equivalent to a controlled object with power controller, and the injected active and reactive power of system is regulated by altering the amplitude and phase of output voltage of system. As the bandwidth of the power control loop is designed to be much slower than the inner voltage/current loop for system stability, and the low equivalent output impedance presented by the system, the phase difference resulting from the grid frequency fluctuation will result in a great change of output current of inverter, which almost leave no time for the power control loop to compensate it and then trip the system. In other word, the DC-GCI's frequency stability is more associated with the voltage tracking ability of its inner voltage/current loop.

Therefore, for more clearly understanding what will influence the system stability when grid frequency fluctuation occurred, the small-signal space state models (SSSM) of system without power controller are established, which means the system is connected with the grid utility only with the synchronous reference frame phase-locked loop (SRF-PLL) and voltage/current inner controller.

A DC-GCI with PI controller in the dq frame

The voltage and phase of the grid utility at PCC is detected by SRF-PLL and its performance will affect the system stability. The equivalent model of SRF-PLL is shown in Fig.4. There is no physical meaning of the state variable τ_{pll}, but it will help to establish the SSSM. The θ is the phase output of SRF-PLL, and the k_{pPLL} and k_{iPLL} are the control parameters of PI controller used in SRF-PLL, v_{gdq} are direct and quadrature grid's voltage at PCC. The SSSM of SRF-PLL is shown following:

$$s\begin{bmatrix}\Delta\tau_{pll}\\ \Delta\theta\end{bmatrix}_{(2x1)} = A_{pll1(2x2)}\begin{bmatrix}\Delta\tau_{pll}\\ \Delta\theta\end{bmatrix}_{(2x1)} + A_{pll2(2x2)}\left[\Delta v_{gdq}\right]_{(2x1)} \quad (3)$$

Where $A_{pll1(2x2)} = \begin{bmatrix}0 & 0\\ 1 & 0\end{bmatrix}_{(2x2)}$, $A_{pll2(2x2)} = \begin{bmatrix}-k_{iPLL} & 0\\ -k_{pPLL} & 0\end{bmatrix}_{(2x2)}$

The state variable of integer in the *dq* frame of PI voltage controller is represented as λ_{dq}. k_{iv} is integer item of voltage controller. The SSSM can be derived according to Fig.5, as shown following:

$$s\left[\Delta\lambda_{dq}\right]_{(2x1)} = B_{v1(2x2)}\left[\Delta v_{gdq}\right]_{(2x1)} - B_{v2(2x2)}\left[\Delta v_{odq}\right]_{(2x1)} \quad (4)$$

Where:

$$B_{v1(2x2)} = \begin{bmatrix}0 & 0\\ 0 & k_{iv}\end{bmatrix}_{(2x2)}, B_{v2(2x2)} = \mathrm{diag}(k_{iv}, k_{iv})$$

Then, the numerical output equation of voltage controller can be represented as:

$$\begin{aligned}\left[\Delta i^{*}_{Ldq}\right]_{(2x1)} &= B_{v3(2x2)}\left[\Delta\lambda_{dq}\right]_{(2x1)} + B_{v4(2x2)}\left[\Delta v_{gdq}\right]_{(2x1)}\\ &\quad - B_{v5(2x2)}\left[\Delta v_{odq}\right]_{(2x1)}\end{aligned} \quad (5)$$

Where:

$$B_{v3(2x2)} = \mathrm{diag}(1,1), B_{v4(2x2)} = \begin{bmatrix}0 & 0\\ 0 & k_{pv}\end{bmatrix}_{(2x2)},$$

$$B_{v5(2x2)} = \mathrm{diag}(k_{pv}, k_{pv})$$

As only the proportional term k_{pi} is adopted in the current controller of inverter, the corresponding numerical output

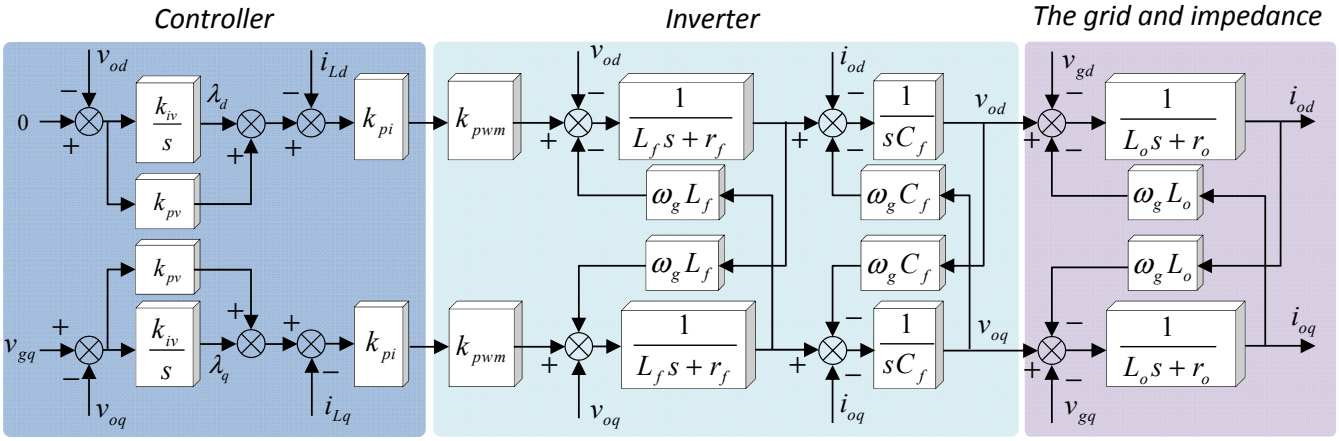

Fig. 5. The control scheme of DC-GCI with PI controller in the *dq* frame

equation can be derived as shown following:

$$\left[\Delta v^{*}_{PWMdq}\right]_{(2\times1)} = C_{i(2x2)}\left[\Delta i^{*}_{Ldq}\right]_{(2\times1)} - C_{i(2x2)}\left[\Delta i_{Ldq}\right]_{(2x1)} \quad (6)$$

Where

$$C_{i(2x2)} = \mathrm{diag}(k_{pi}, k_{pi})$$

According to (5), (6) and Fig.5, the SSSM of inductor of filter can be derived in (7), in which the parameters of r_f and L_f are resistance and inductance of inductor respectively, k_{PWM} is equivalent proportion coefficient of inverter, ω_g is grid frequency.

$$\begin{aligned} s\left[\Delta i_{Ldq}\right]_{(2x1)} &= (G_{1(2x2)} - G_{3(2x2)}C_{i(2x2)})\left[\Delta i_{Ldq}\right]_{(2x1)} \\ &+(G_{2(2x2)} - G_{3(2x2)}C_{i(2x2)}B_{v5(2x2)})\left[\Delta v_{odq}\right]_{(2x1)} \\ &+G_{3(2x2)}C_{i(2x2)}B_{v3(2x2)}\left[\Delta\lambda_{dq}\right]_{(2x1)} \\ &+G_{3(2x2)}C_{i(2x2)}B_{v4(2x2)}\left[\Delta v_{gdq}\right]_{(2x1)} \end{aligned} \quad (7)$$

Where:

$$G_{1(2x2)} = \begin{bmatrix} -\frac{r_f}{L_f} & \omega_g \\ -\omega_g & -\frac{r_f}{L_f} \end{bmatrix}_{(2x2)}, G_{2(2x2)} = \mathrm{diag}(-\frac{1}{L_f}, -\frac{1}{L_f}),$$

$$G_{3(2x2)} = \mathrm{diag}(\frac{k_{PWM}}{L_f}, \frac{k_{PWM}}{L_f})$$

In the same way, the SSSM of capacitor of filter is shown in (8), in which the capacitance of the capacitor is represented as C_f.

$$\begin{aligned} s\left[\Delta v_{odq}\right]_{(2x1)} &= G_{4(2x2)}\left[\Delta v_{odq}\right]_{(2x1)} + G_{5(2x2)}\left[\Delta i_{Ldq}\right]_{(2x1)} \\ &-G_{5(2x2)}\left[\Delta i_{odq}\right]_{(2x1)} \end{aligned} \quad (8)$$

Where:

$$G_{4(2x2)} = \begin{bmatrix} 0 & \omega_0 \\ -\omega_0 & 0 \end{bmatrix}_{(2x2)}, G_{5(2x2)} = diag(\frac{1}{C_f}, \frac{1}{C_f})$$

The injected active and reactive of DC-GCI is resulting from the different phase and amplitude of voltage between the line impedance. Therefore, the SSSM of this part is shown in (9), in which the r_o and L_o are resistance and inductance of line impedance respectively

$$\begin{aligned} s\left[\Delta i_{odq}\right]_{(2x1)} &= G_{6(2x2)}\left[\Delta i_{odq}\right]_{(2x1)} + G_{7(2x2)}\left[\Delta v_{odq}\right]_{(2x1)} \\ &-G_{7(2x2)}\left[\Delta v_{gdq}\right] \end{aligned} \quad (9)$$

Where:

$$G_{6(2x2)} = \begin{bmatrix} -\frac{r_o}{L_o} & \omega_0 \\ -\omega_0 & -\frac{r_o}{L_o} \end{bmatrix}_{(2x2)}, G_{7(2x2)} = diag(\frac{1}{L_o}, \frac{1}{L_o})$$

Above all, the complete SSSM of DC-GCI with PI voltage controller and SRF-PLL in the *dq* frame can be represented in (10), of which the details are shown in (11).

$$\begin{cases} s\Delta x_{sys} = A_{sys}\Delta x_{sys} + B_{sys}\left[\Delta v_{gdq}\right]_{(2x1)} \\ \Delta y_{sys} = C_{sys}\Delta x_{sys} \end{cases} \quad (10)$$

It can be seen that the system's SSSM is multiple input and multiple output (MIMO) system. Therefore, the matrix of transfer function can be derived as shown following:

$$\begin{bmatrix} G^{Vgd}_{iod}(s) & G^{Vgq}_{iod}(s) \\ G^{Vgd}_{ioq}(s) & G^{Vgq}_{ioq}(s) \end{bmatrix} = C_{sys}(sI - A_{sys})^{-1}B_{sys} \quad (12)$$

The steady value of output direct and quadrature current of system (I_{odq}) after a grid voltage step up disturbance in the *dq* frame can be derived through the final value theorem of the Laplace transform, as shown in (13), in which the ΔV_{gdq} is the amplitude of step up disturbance voltage of the grid.

$$x_{sys} = \left[\Delta\tau_{pll} \quad \Delta\theta \quad \Delta\lambda_{dq} \quad \Delta i_{Ldq} \quad \Delta v_{odq} \quad \Delta i_{odq}\right]^{T}_{(1x10)}$$

$$A_{sys} = \begin{bmatrix} A_{pll1(2x2)} & 0_{(2x2)} & 0_{(2x2)} & 0_{(2x2)} & 0_{(2x2)} \\ 0_{(2x2)} & 0_{(2x2)} & 0_{(2x2)} & -B_{v2(2x2)} & 0_{(2x2)} \\ 0_{(2x2)} & G_{3(2x2)}C_{i(2x2)}B_{v3(2x2)} & G_{1(2x2)} - G_{3(2x2)}C_{i(2x2)} & G_{2(2x2)} - G_{3(2x2)}C_{i(2x2)}B_{v5(2x2)} & 0_{(2x2)} \\ 0_{(2x2)} & 0_{(2x2)} & G_{5(2x2)} & G_{4(2x2)} & -G_{5(2x2)} \\ 0_{(2x2)} & 0_{(2x2)} & 0_{(2x2)} & G_{7(2x2)} & G_{6(2x2)} \end{bmatrix}_{(10x10)} \quad (11)$$

$$, B_{sys} = \begin{bmatrix} A_{pll2(2x2)} \\ B_{v1(2x2)} \\ G_{3(2x2)}C_{i(2x2)}B_{v4(2x2)} \\ 0_{(2x2)} \\ -G_{7(2x2)} \end{bmatrix}_{(10x2)}, C_{sys} = \begin{bmatrix} 0_{(2x8)} & 1 & 0 \\ & 0 & 0 \end{bmatrix}_{(2x10)}$$

$$\begin{cases} \Delta I_{od} = \lim\limits_{s\to 0} \Delta V_{gd}(s) G_{iod}^{Vgd}(s) + \lim\limits_{s\to 0} \Delta V_{gq}(s) G_{iod}^{Vgq}(s) \\ \Delta I_{oq} = \lim\limits_{s\to 0} \Delta V_{gd}(s) G_{ioq}^{Vgd}(s) + \lim\limits_{s\to 0} \Delta V_{gq}(s) G_{ioq}^{Vgq}(s) \end{cases} \tag{13}$$

Then, the impact of ω_g to the system can be evaluated by the sensitivity analysis, as shown following:

$$\begin{cases} \dfrac{\partial \Delta I_{do}}{\partial \omega_g} = \dfrac{2L_o^2 r_o \Delta V_{gd} \omega_g}{(r_o^2 + L_o^2 \Delta \omega_g^2)^2} \\ \dfrac{\partial \Delta I_{qo}}{\partial \omega_g} = -\dfrac{2L_o^3 \Delta V_{gd} \omega_g^2}{(r_o^2 + L_o^2 \omega_g^2)^2} + \dfrac{L_o \Delta V_{gd}}{r_o^2 + L_o^2 \omega_g^2} \end{cases} \tag{14}$$

The relationship between $\partial I_{odq}/\partial \omega_g$ and ω_g are shown in Fig. 6(a.1) and Fig. 6(b.1). It can be seen that grid's frequency fluctuation have almost no influence on the inverter's grid-connecting current when PI voltage controller is adopted by the system in the *dq* frame.

B DC-GCI with PR controller in the ab frame

As there is no analytical solution to the system error transfer function with the disturbance of the sine/cosine signals in the Laplace domain, the PR controllers are usually used in DC-GCI for tracking the reference without error in $\alpha\beta$ frame. In order to derive the similar transfer function matrix for i_{odq}, the SSSM for PR controller in the *dq* frame is established firstly, as shown in(15) and Fig.7.

$$\begin{cases} s x_{pr} = A_{pr} x_{pr} + B_{pr} u \\ y_{pr} = C_{pr} x_{pr} \end{cases} \tag{15}$$

Where,

$$x_{pr} = \begin{bmatrix} \alpha_d & \alpha_q & \beta_d & \beta_q \end{bmatrix}^T,$$

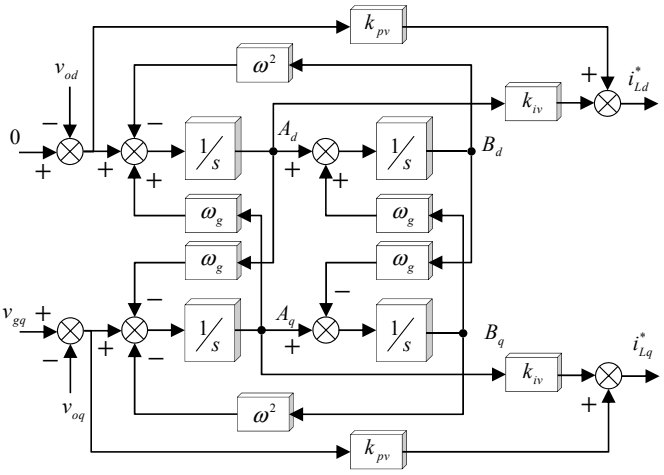

Fig. 7. The equivalent model of PR controller in the *dq* frame

$$A_{pr} = \begin{bmatrix} 0 & \omega_g & -\omega^2 & 0 \\ -\omega_g & 0 & 0 & -\omega^2 \\ 1 & 0 & 0 & \omega_g \\ 0 & 1 & -\omega_g & 0 \end{bmatrix}, B_{pr} = \begin{bmatrix} 1 & 0 \\ 0 & 1 \\ 0 & 0 \\ 0 & 0 \end{bmatrix},$$

$$C_{pr} = \begin{bmatrix} 1 & 0 & 0 & 0 \\ 0 & 1 & 0 & 0 \end{bmatrix}$$

In the same way, the complete small signal state space model of DC-GCI with fixed or dynamic resonant frequency PR voltage controller can be established with state variable of $x_{sys(12x1)} = \begin{bmatrix} \Delta\tau_{pll} & \Delta\theta & \Delta\alpha_{dq} & \Delta\beta_{dq} & \Delta i_{Ldq} & \Delta v_{odq} & \Delta i_{odq} \end{bmatrix}^T_{(1x12)}$.

Then, the relationship between $\partial I_{odq}/\partial \omega_g$ and ω_g when fixed resonant frequency based PR voltage controller is adopted are shown in the Fig. 6(a.2) and Fig. 6(b.2). It can be seen that the direct and quadrature current of system will be

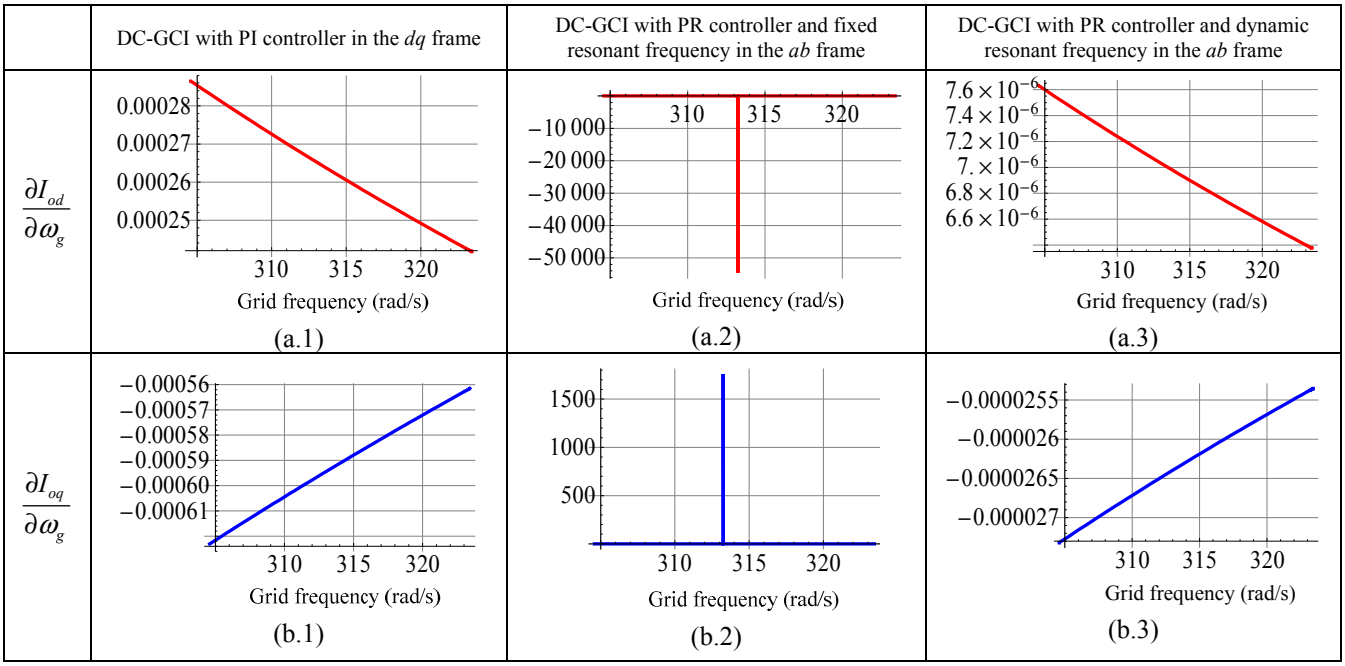

Fig. 6. The comparison sensitivity analysis of the system with different voltage control strategies.

affected seriously by the deviation of grid frequency. Although the complete system may have a chance to be stabilized, more bandwidth is needed to make the power controller to work quickly, it means the bandwidth difference between voltage and power control loop is decrease, and this will deteriorate the system's stability.

On the contrary, the influence will be improved when the resonant frequency of PR voltage controller is changing according to the grid's frequency fluctuation, namely the output of SRF-PLL, as shown in Fig. 6(a.3) and Fig. 6(b.3). That is because the performance of PR controller will be maintained regardless frequency operation point changing. In summary, the DC-GCI with PI voltage controller in the *dq* frame or dynamic resonant frequency based PR voltage controller in the *ab* frame is more suitable and easy to control for the islanded MG.

IV. The Simulation and Experiment Verification

A The simulation verification

In order to verify the comparing result from theoretical analysis, the simulation model is built in the Matlab/Simulink, which is consisting of the ideal grid utility and a 2 kW DC-GCI. The stability of the system with different inner voltage control strategy when the grid frequency disturbance occurred is tested based on the same scenario. The control and power stage parameters are shown in Tab I.

TABLE I
THE PARAMETERS OF SIMULATION

	Parameters		Value
		Description	
Common parameters	k_{pPLL}	PLL proportional term	141.1
	k_{iPLL}	PLL integral coefficient	10000
	P^*	Active power reference	400 W
	Q^*	Reactive power reference	0 var
	L_f	Filter inductance	1.5 mH
	r_f	Filter resistance	0.1 Ω
	C_f	Filter capacitance	9 μF
	L_o	Line inductance	1.5 mH
	r_o	Line resistance	0.1 Ω
	ω_0	Time constant of LPF	50
	k_{pwm}	Inverter equivalent constant	200
	$f_{disturb}$	Grid frequency disturbance	2.5 Hz
	$Load_1$	Sensitive loads	340 W
	$Load_2$	Regular loads	670 W
Control in the *dq* frame	k_{pv}	Voltage proportion item	0.01
	k_{iv}	Voltage integration item	1
	k_{pi}	Current proportion item	0.5
	k_{pP}	Active power proportion item	1.5e-4
	k_{iP}	Active power integration item	1e-5
	k_{dP}	Active power differential item	7e-6
	k_{pQ}	Reactive power proportion item	1e-2
	k_{iQ}	Reactive power integration item	1e-4
	k_{dQ}	Reactive power differential item	7e-5
Control in the *ab* frame	k_{pv}	Voltage proportion item	0.053
	k_{iv}	Voltage resonant item	3.24
	k_{pi}	Current proportion item	0.603
	k_{pP}	Active power proportion item	1e-5
	k_{iP}	Active power integration item	2e-5
	k_{dP}	Active power differential item	1e-6
	k_{pQ}	Reactive power proportion item	1e-3
	k_{iQ}	Reactive power integration item	2e-4
	k_{dQ}	Reactive power differential item	1e-6

The inverter is connected with the grid utility at PCC through line impedance. As there is integration item in power loop of the DC-GCI, it can be seen that there is no error between the power reference and injected active and reactive power. Although the parameters of power controller are different with each control strategies, the system is already in the steady state before grid frequency step up disturbance of 2.5 Hz occurred at 100 s.

It can be seen from the Fig.8 that the injected active and reactive power of inverter adopted PI controller in the *dq* frame in voltage control loop is almost not affected by the grid frequency disturbance. The greatest deviation of active and reactive power in dynamic response is around 5 W and 7 var

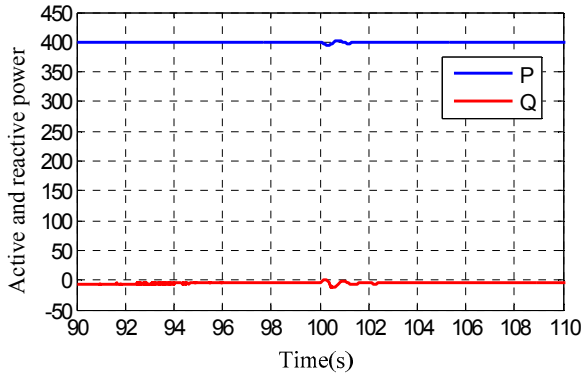

Fig. 8. The simulation of injected active/reactive power of system with PI voltage controller in the *dq* frame.

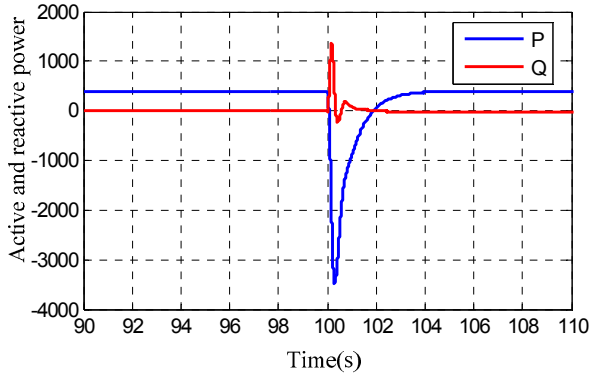

Fig. 9. The simulation of injected active/reactive power of system with fixed resonant frequency PR voltage controller in the *ab* frame.

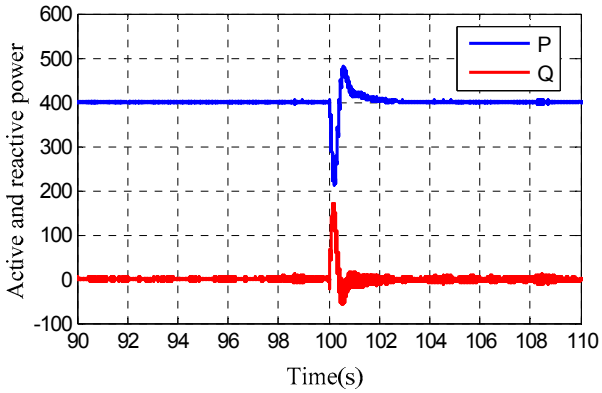

Fig. 10 The simulation of injected active/reactive power of system with dynamic resonant frequency PR voltage controller in the *ab* frame.

respectively. However, when the fixed resonant frequency based PR controller is adopted by DC-GCI in the *ab* frame as voltage controller, the system's output power is affected by the grid's frequency change severely, as shown in Fig.9. Although the system is finally stabilized by the power control controller after the dynamic response, the peak value of active and reactive in dynamic is around -3400 W and 1300 var. Obviously, this will trip the inverter in practice more easily, and make it more difficult to design the system's power controller.

On the contrary, the output power dynamic response of the system is improved when the PR controller's fixed resonant frequency is replaced by dynamic resonant frequency generated by SRF-PLL, as shown in Fig.10. The peak value of active and reactive power under grid's frequency disturbance is decreased to around 210 W and 180 var.

B The experiment verification

At same time, for verifying the analysis result, a scaled-down experimental setup consisting of two Danfoss 2.2 kW inverters, a real-time dSPACE1006 platform, *LC* filters, line impedance, and two resistive loads has been built, as shown in Fig.11. One inverter is used for emulating the grid utility with frequency step up disturbance, while the other one is controlled as the DC-GCI with different inner voltage/current control strategy. $Load_1$ is sensitive loads supplied by DC-GCI and $Load_2$ is supplied by the grid. The voltage of DC link is 650V and the AC bus's voltage is set to 230V, the switching frequency of controller is set to 10 kHz.

In the same way, the inverter with DC-GCI control strategy is already connected to the emulated grid, and the dispatched active and reactive power is controlled by power controller to inject into the emulated grid in steady state before the frequency step up disturbance testing in the experiment, as shown in Fig. 12(a).

As the frequency/phase of the grid utility at PCC detected by SRF-PLL is used in the Park transform when PI voltage controller is adopted by the inverter. It can be seen from Fig.

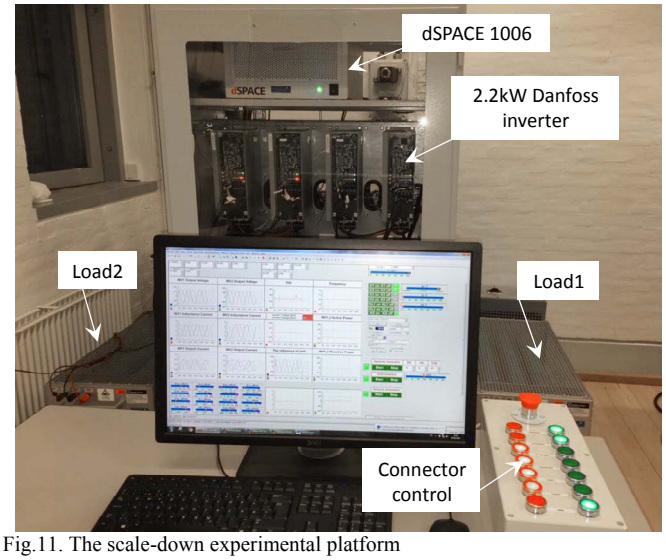

Fig.11. The scale-down experimental platform

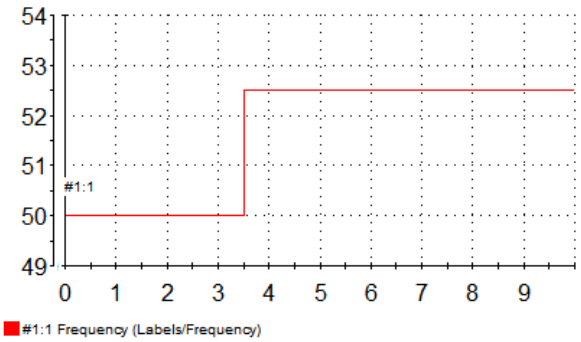

(a) The grid's frequency

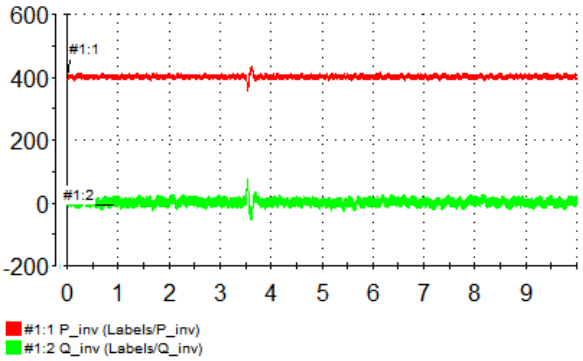

(b) The injected active and reactive power

Fig. 12. The experiment of injected active/reactive power of system with PI voltage controller in the *dq* frame.

12(b) that the DC-GCI can overcome the influence resulting from grid's frequency or phase step up disturbance inherently and the power dynamic response is compensated by power controller only with tiny fluctuation, which is in accordance with the parameter sensitive analysis and simulation above.

However, the DC-GCI is tripped by overcurrent as shown in Fig. 13 when comparing to Fig. 9. That is because that the attenuation of voltage tracking ability of the inner voltage and current loop, which resulting from frequency operation point deviation and the feature of fixed resonant frequency based PR controller, cannot be compensated by power controller in time.

The Fig. 14 describes the power response of DC-GCI with dynamic resonant frequency based PR voltage controller under the same disturbance. As the resonant frequency of controller

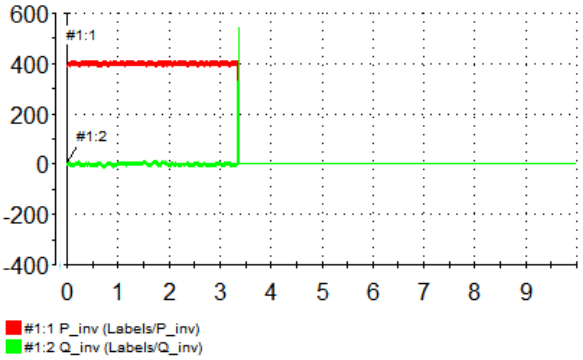

Fig. 13. The experiment of injected active/reactive power of system with fixed resonant frequency PR voltage controller in the *ab* frame.

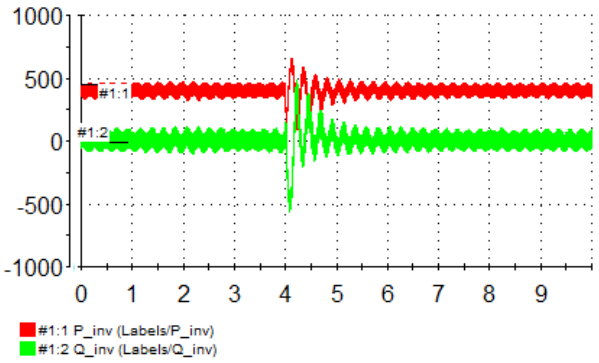

Fig. 14. The experiment of injected active/reactive power of system with dynamic resonant frequency PR voltage controller in the *ab* frame.

is adjusted according to the grid's frequency, the feature of resonant controller is maintained. Although there is more power oscillation when comparing to the system with PI voltage controller in the *dq* frame, the system can still get back to the stable point after the disturbance.

V. Conclusion

For analyzing and estimating the impact of grid's frequency fluctuation to the stability of DC-GCI in the islanded MG, the small signal state space model of the system with three widely used inner voltage/current control schemes have been established and compared. The conclusion is derived from the parameter sensitivity analysis of the system state matrix and grid's frequency, it shown that the DC-GCI with PI voltage controller in the *dq* frame or dynamic resonant frequency based PR controller in the *ab* frame can overcome the grid frequency disturbance inherently, and this conclusion will also facilitate the power loop controller designing when connecting DC-GCI to the small scale or islanded MG. Finally, the validity is verified through the simulation and experiment.

Acknowledgement

The authors would like to appreciate the supports by the National International Science & Technology Cooperation Project (2014DFG62610), the National High Technology Research and Development Program (863 Program, 2015AA050606), and the Key Project of The Natural Science Foundation of Beijing (KZ201511232035).

References

[1] R. Lasseter, A. Akhil, C. Marnay, J. Stevens, et al, "The certs microgrid concept - white paper on integration of distributed energy resources," Technical Report, U.S. Department of Energy, 2002.

[2] Blaabjerg, F., Zhe Chen, Kjaer, S.B, "Power electronics as efficient interface in dispersed power generation systems," IEEE Transactions on Power Electronics, vol.2, no.2, pp. 1184-1194, 2004

[3] Nikos Hatziargyriou, Hiroshi Asano, Reza Iravani, etc, "Microgrid," IEEE power & energy magazine, vol. 5, no.4, pp. 78-94, 2007

[4] Guerrero, J.M.; Chandorkar, M.; Lee, T.; Loh, P.C., "Advanced Control Architectures for Intelligent Microgrids-Part I: Decentralized and Hierarchical Control," IEEE Transactions on Industrial Electronics, vol. 60, no.4, pp. 1254 – 1262, 2013

[5] Qobad Shafiee, Josep M. Guerrero, Juan C. Vasquez, "Distributed secondary control for islanded MicroGrids - A networked control systems approach," IEEE Transactions on Power Electronics, vol. 29,no.2, pp 5637 – 5642, 2014

[6] Yu Xiao, KhambadkoneA M, Wang Huan, et al. "Control of Parallel-Connected power converters for Low-Voltage microgrid—part i: a hybrid control architecture," Power Electronics, IEEE Transactions on, vol.25, no.12, pp., 2962-2970. 2010.

[7] S. B. Kjaer; J. K. Pedersen; F. Blaabjerg. "A review of single-phase grid-connected inverters for photovoltaic modules," IEEE Transactions on Industry Applications, vol.41, no.5, pp., 1292-1306. 2005.

[8] J. H. R. Enslin; P. J. M. Heskes , "Harmonic interaction between a large number of distributed power inverters and the distribution network," IEEE Transactions on Power Electronics, vol.19, no. 6, pp. 1586-1593, 2004.

[9] J. He and Y. W. Li, "Hybrid voltage and current control approach for DG grid interfacing converters with LCL filters," IEEE Transactions on Industrial Electronics, vol.60, no.5, pp. 1797-1809, 2013.

[10] Jinwei He, Edmonton AB, Yun Wei Li, et al, "Investigation and resonances damping of multiple PV inverters," APEC2012, Orlando, 2012.

[11] Wei. Feng, Kai. Sun, Yajuan. Guan, J.M. Guerrero, Xi. Xiao, "A harmonic current suppression control strategy for droop-controlled inverter connected to the distorted grid," Energy Conversion Congress and Exposition (ECCE), Montreal, QC, 2015.

[12] J. He and Y. W. Li. Flexible microgrid power quality enhancement using adaptive hybrid voltage and current controller [J]. IEEE Transactions on Industrial Electronics, 2014, 61(6): 2784-2794.

[13] WEI Shouping. Analysis and Simulation on the Primary Frequency Regulation and Isolated Grid Operation Characteristic of Hydraulic Turbine Regulation System[J]. Hydropower Automation and Dan Monitoring, 2009, 33(6):27-39.

[14] Prabha Kunder, Power Stability and Control, 1st ed., McGraw-Hill, 1994.

[15] Y. Guan; J. M. Guerrero; X. Zhao; J. C. Vasquez; X. Guo, "A New Way of Controlling Parallel-Connected Inverters by Using Synchronous-Reference-Frame Virtual Impedance Loop—Part I: Control Principle," IEEE Transactions on Power Electronics, vol.31, No.6, pp. 4576–4593, 2016.

[16] Xiongfei Wang, Josep M. Guerrero, Frede Blaabjerg, etc, "Secondary voltage control for harmonics suppression in islanded microgrids," Power and Energy Society General Meeting IEEE, San Diego, CA, 2011.